Ab initio study of the surface properties and ideal strength of (100) silicon thin films

Yoshitaka Umeno,[1,2,*] Akihiro Kushima,[2] Takayuki Kitamura,[2] Peter Gumbsch,[1,3] and Ju Li[4]
[1]*IZBS, University of Karlsruhe, Kaiserstrasse 12, 76131 Karlsruhe, Germany*
[2]*Graduate School of Engineering, Kyoto University, Sakyo-ku, Kyoto 606-8501, Japan*
[3]*Fraunhofer IWM, Wöhlerstrasse 11, 79108 Freiburg, Germany*
[4]*Department of Materials Science and Engineering, Ohio State University, Columbus, Ohio 43210, USA*
(Received 2 June 2005; revised manuscript received 23 August 2005; published 31 October 2005)

Studying the ideal strength of nanostructured materials is important for understanding of their mechanical properties. We have performed *ab initio* modeling of nanoscale Si films with (100) surfaces and computed the surface energy and surface stress as well as the ideal tensile strength of the structure. The strength of the thin film is not significantly decreased down to a thickness of less than 1 nm. Surprisingly, there is also no considerable effect of the surface reconstruction. This suggests that the lower stresses found for surface crack nucleation in an experiment are due to substantial flaws and not an intrinsic effect of the ideal surface. The band gap energy of the thin film is lower than that of the bulk, but a band gap remains up to high strain in the thin film.

DOI: 10.1103/PhysRevB.72.165431 PACS number(s): 68.35.Gy, 31.15.Ar, 62.25.+g

I. INTRODUCTION

Understanding the strength of materials from microscopic scale is essential for materials mechanics. Multiscale modelling for this issue has revealed that the behavior of materials in atomistic and/or electronic scale can play an important role in the mechanical properties.[1–6] Moreover, with the advent of nanotechnology and materials structured on the nanometer scale, there is increasing interest in the microscopic understanding of the mechanical properties of such scales.[7,8] Therefore, systematic investigations of the effect of the nanoscale structure on the mechanical properties of components are needed.

The ideal (theoretical) strength, which is, in general, defined for a perfect crystal subject to a uniform deformation as the stress at which an unstable deformation takes place, was originally discussed using simple interatomic potential.[9–11] Since the ideal strength, which is the highest attainable stress of the material, is a fundamental mechanical property, a lot of studies for various crystals have been performed, employing not only empirical potential[12–21] but also first principles (*ab initio*) methodology.[22–28] Through these efforts the ideal strength of perfect crystals has been well investigated.

Studying a perfect crystal is interesting and sets the limits but is certainly not sufficient for the clarification of the mechanical properties of real structured materials. The strength of materials is sensitive to their structure. It is therefore required to investigate the effect of the structure on the mechanical properties. As a first step we can consider structures with high symmetry. For this it is straightforward to expand the definition of the ideal strength to include the strength at instability of components with ideal structures. That is, we define the attainable stress of structured material as "ideal structural strength," and conduct precise evaluation by *ab initio* calculations.

In this study, we investigate tensile deformation of silicon nanoscale thin films with the aim to clarify the ideal structural strength of a surface. We carry out *ab initio* tensile simulations for freestanding silicon thin films with (100) surfaces and obtain their ideal structural strengths. The dependence of the strength on the tensile direction is investigated. Furthermore, density of states of the nanofilms under deformation is examined.

II. SIMULATION PROCEDURE

A. Simulation method

First-principles (*ab initio*) simulations for tensile deformation of silicon nanometer thin films (nanofilms) are performed. We use VASP (Vienna Ab-initio Simulation Package[29,30]) for the first-principles calculations, which is a DFT (Density Functional Theory[31–33]) simulation package using a plane-wave basis set with ultrasoft pseudopotentials.[34] The cut-off energy of the plane waves is 300 eV. The exchange-correlation energy is evaluated by GGA using the Perdew-Wang function.[35]

The validity of the methodology has been preliminarily confirmed by evaluating the properties of the bulk. For example, the calculated lattice constant is 0.5457 nm (0.543 nm[36]), Young's modulus is 167 GPa (169 GPa[37]), elastic constants are $C_{11}=154$ GPa (168 GPa[38]), $C_{12}=55$ GPa (65 GPa[38]), $C_{111}=-839$ GPa (−825 GPa[39]), $C_{112}=-5.1$ (−4.8 GPa[39]). In the parentheses are experimental values in the literature. The good agreement up to the third-order elastic constants supports the validity of the methodology we employ.

B. Relaxation and tensile simulation

Figure 1 shows simulation models for silicon nanofilms. Initially the atoms are arranged on the lattice points of the diamond structure with the lattice constant, a, of 0.5457 nm, then the atomic configuration is relaxed with the conjugate gradient method to have the $p(2\times1)$ asymmetric surface structure. The relaxed structures, where the normal stresses in the x and y directions, σ_{xx} and σ_{yy}, are zero, are shown in the figure and discussed later. The k-point grids in the Bril-

 ©2005 The American Physical Society

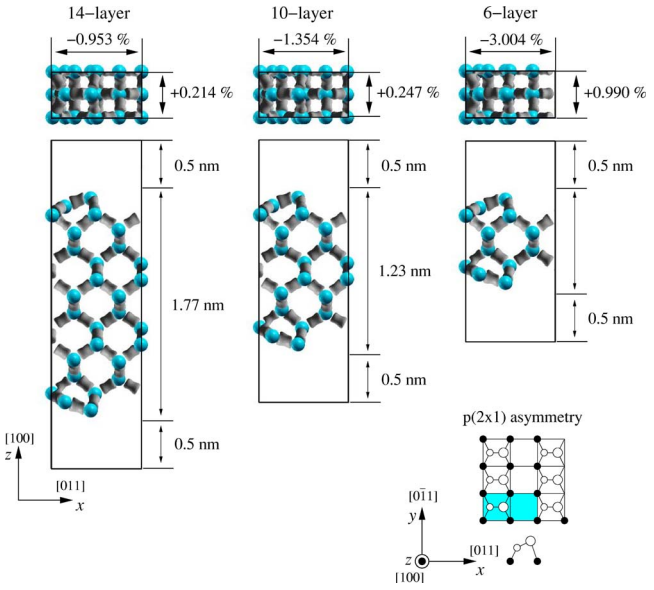

FIG. 1. (Color online) Simulation models of Si nanofilms. The initial strain due to surface relaxation is marked in% in the top view figures. Dimensions perpendicular to the surface after the relaxation (vacuum region and distance between the top and the bottom atoms) are indicated in nm.

louin zone selected according to the Monkhorst-Pack method[40] are $5\times9\times2$, $5\times9\times2$, and $9\times15\times3$ for 14-layer, 10-layer, and 6-layer models, respectively. Uniaxial strain is applied stepwise in the x direction, ε_{xx}, with an increment of $\Delta\varepsilon$. The structure is fully relaxed at each strain under the free transverse-stress condition, $\sigma_{yy}=0$, to mimic geometrically the unconstrained tensile condition. The simulation of tension in the y direction is also conducted for the 14-layer model in the same manner.

III. RESULTS

A. Relaxed structure, effective film thickness

Figure 1 shows the relaxed atomic configurations of the thin film models.[41] The bond structures are also depicted in the figure by the cylinders that are drawn by the isosurface with the charge density of 0.425×10^3 nm^{-3}. The thickness and the length of the isocharge cylinders are almost the same both in the bulk and at the surfaces, meaning that the charge density is distributed equally.

Before one can compute the stress-strain curves of a thin film one has to face the following question: what is the thickness of the film? In macroscopic discussions this question is trivial, microscopically the thickness of the surface layer matters and requires specific treatment. The approach followed here takes a thermodynamics view in which the surface stress is balanced by bulk stress of a film of finite thickness. If all moduli, surface stresses and their derivatives are collected independently, the picture may be used to derive a definition of film thickness.

Changes in the simulation box size from the initial dimensions of the lattice, L_x and L_y, which are 0.772 and 0.386 nm, respectively, due to the presence of the surface and due to surface reconstruction are indicated in Fig. 1. The surface reconstruction induces contraction in the x direction ([011]) and expansion in y ([0$\bar{1}$1]) because of the arrangement of the dimer rows of the $p(2\times1)$ asymmetric surface structure.

Surface stress effects on the isotropic compression of a thin film have been discussed by Cammarata *et al.*[42,43] based on a thermodynamic analysis. Here we extend their discussion to the anisotropic case and derive

$$t_0[1-\nu'(\varepsilon_x+\varepsilon_y)]\left[E'_{xx0}\left(\varepsilon_x-\frac{1}{2}B'_{xx}\varepsilon_x^2\right)+E'_{xy0}\left(\varepsilon_y-\frac{1}{2}B'_{xy}\varepsilon_y^2\right)\right]+2f_{x0}+2\left(\frac{\partial f_x}{\partial\varepsilon_x}\right)_0\varepsilon_x+2\left(\frac{\partial f_x}{\partial\varepsilon_y}\right)_0\varepsilon_y=0, \quad (1)$$

$$t_0[1-\nu'(\varepsilon_x+\varepsilon_y)]\left[E'_{yy0}\left(\varepsilon_y-\frac{1}{2}B'_{xx}\varepsilon_y^2\right)+E'_{yx0}\left(\varepsilon_x-\frac{1}{2}B'_{yx}\varepsilon_x^2\right)\right]+2f_{y0}+2\left(\frac{\partial f_y}{\partial\varepsilon_y}\right)_0\varepsilon_y+2\left(\frac{\partial f_y}{\partial\varepsilon_x}\right)_0\varepsilon_x=0, \quad (2)$$

where $E'_{xx}(=E'_{yy})$, $E'_{xy}(=E'_{yx})$, $B'_{xx}(=B'_{yy})$, $B'_{xy}(=B'_{yx})$, and ν' are the elastic properties of the bulk when infinitesimal deformation in the x direction ([011]) is applied while the stress only in the z axis ([100]) is null; i.e., strain in the y axis ([0$\bar{1}$1]) is constraint. E' is the second-order elastic modulus, $\sigma=E'\varepsilon$, B' is the ratio between the third- and second-order elastic modulus, $B'=-(\partial E'/\partial\varepsilon)/E'$, and ν' is the ratio of the strains, $\nu'=-\varepsilon_z/\varepsilon_x$. The bulk Si values are $E'_{xx}(=E'_{yy})=161.1$ GPa, $B'_{xx}(=B'_{yy})=4.26$, $B'_{xy}(=B'_{yx})=6.34$, and $\nu'=0.359$. ε_x and ε_y are the strains due to the surface stress, f_x and f_y are the surface stresses of Si(100) surface (i.e., $f_x=\partial\gamma_L/\partial\varepsilon_x$, γ_L is the Lagrangian surface energy). The subscript naught stands for the values of the equilibrium state. The surface stresses and their derivatives are calculated numerically from the the surface energy as a function of the strain, which is obtained by applying small strain, ε_{xx} and ε_{yy}, to the thin films. The obtained values are listed in Table I. Substituting these constants and the values of deformation due to surface stress (in Fig. 1) into Eq. (1), the thickness of the films, t_0, can be evaluated. The so-estimated thickness is

TABLE I. Surface stress and its derivative of Si(100) (N/m).

	f_{x0}	f_{y0}	$\left(\frac{\partial f_x}{\partial\varepsilon_x}\right)_0$	$\left(\frac{\partial f_y}{\partial\varepsilon_y}\right)_0$	$\left(\frac{\partial f_x}{\partial\varepsilon_y}\right)_0$	$\left(\frac{\partial f_y}{\partial\varepsilon_x}\right)_0$
This work	1.284	−0.286	−25.0	−33.0	−5.44	−10.6
Ref. 47	1.105	−0.401	—	—	—	—

TABLE II. Nominal thickness of thin film, thickness evaluated from thermodynamics by Eq. (1), and mechanical thickness. (Nominal thickness is the number of all atomic layers times one-layer thickness. Mechanical thickness is for the atomic layers excluding the dimer layers. Details in text.)

	14-layer	10-layer	6-layer
Nominal	1.910 nm	1.364	0.819
Eq. (1)	1.949 nm	1.441	0.774
Mechanical	1.637 nm	1.091	0.546

listed in Table II together with nominal and mechanical thicknesses. The nominal thickness is calculated by the number of atomic layers times the thickness of a layer, which is assumed to be equal to the interlayer distance of (100) atomic planes in the bulk, $a/4$. The mechanical thickness is explained and discussed in the next section. Hereafter in this section the stress of the thin films is evaluated using the thermodynamics thickness. Thickness of the initial unstrained configuration is used throughout the deformation process, i.e., nominal stress is used.

B. Tensile simulation in [011] direction

Figure 2 displays tensile stress-strain curves of the silicon nanofilms. The result of the single crystal is also shown. Young's moduli of the films, which is calculated by the initial inclination of the stress-strain curve, are listed in Table III. The stresses in the models change smoothly with the increase of the strain, although the thicknesses of the films are only within 2.0 nm. The ideal strengths (maximum stresses) are also listed in Table III. Obviously stiffness and strength decrease with decreasing film thickness.

Figure 3 shows changes in atomic and electronic configurations in the thin films under tension. For 14- and 10-layer models only the top half of the models are shown. In the 14- and 10-layer models, bond thinning is exhibited at site α first (ε=0.10), followed by thinning at β (ε=0.15). Interestingly, in spite of the changes in the interatomic bonds the 14-layer model shows nearly homogeneous deformation that is similar to that of the bulk. In the 10-layer model, it is observed that the thinning of the bonds propagates inward from site β and causes fracture with bond breaking along the dashed curve in the figure. The 6-layer model gives bond breaking along the dashed straight line. This is apparently due to the bond breaking at site α (and α').

C. Tension in [0$\bar{1}$1] direction

Figure 4 shows the stress as a function of the strain in the 14-layer model under tension in the [011] direction. The results of the bulk and the 14-layer film in the [011] tension are

TABLE III. Young's modulus and ideal strength under [011] tension.

	Bulk	14-layer	10-layer	6-layer
Young's modulus	168 GPa	145.4	131.6	112.4
Ideal strength	15.8 GPa	12.8	10.71	9.45

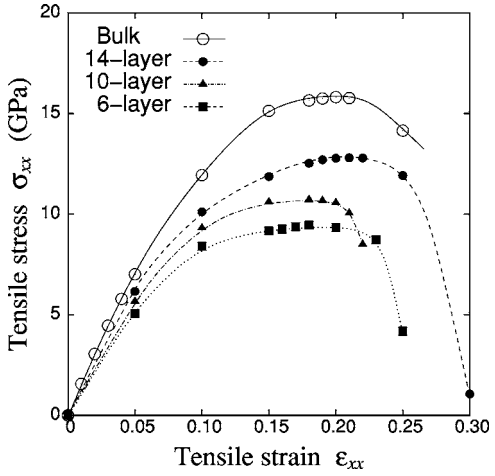

FIG. 2. Tensile stress-strain curves of Si nanofilms in [011] tension.

shown for a comparison. The ideal tensile strength in the [011] direction is 12.96 GPa, which is close to that in the [011] direction (12.80 GPa). However, the decrease in the stress-strain curve occurs at smaller tensile strain, ε_{yy}=0.18, compared to that in [011], ε_{xx}=0.21.

Figure 5 depicts the deformation that changes the surface structure from asymmetric to symmetric between ε_{yy}=0.18 and 0.20, which corresponds to the drop in the stress-strain curve. While the energy of the thin film with the strain of ε_{yy}=0.18 is only slightly lower than that with ε_{xx}=0.18 by 0.071 eV, the energy difference is increased to 0.307 eV at the strain of 0.22. This indicates the change of the dimer shape decreases the energy, which means that the thin film under high tension in [0$\bar{1}$1] direction favors the symmetric dimer structure. Although the tensile stress sustains at about 11.5 GPa after the drop up to ε_{yy}=0.25 followed by the second drop, the thin film immediately leads to the fracture at

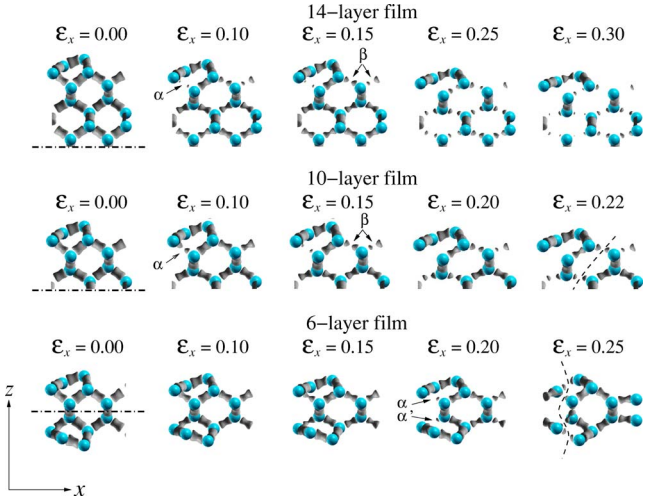

FIG. 3. (Color online) Change in atomic configuration and charge density distribution in Si nanofilms under [011] tension. Only the top half of the system is shown for 14- and 10-layer models.

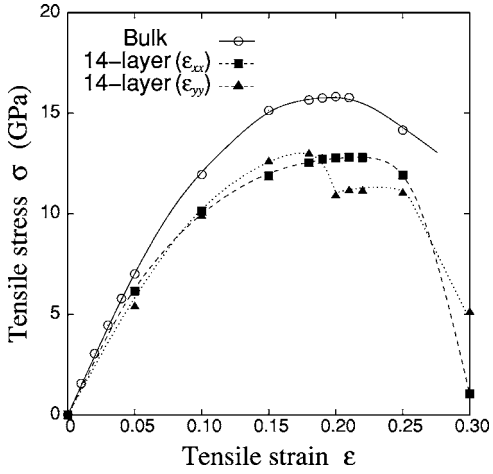

FIG. 4. Tensile stress-strain curves of Si nanofilms in $[0\bar{1}1]$ tension (ε_{yy}). [011] tension (ε_{xx}) and bulk behavior are shown for comparison.

$\varepsilon_{yy}=0.18$ with the bond breaks along the dashed lines under tensile deformation with stress-controlled condition.

D. Change in electronic property under deformation

The density of states for the whole system under the deformation of [011] tension is evaluated for each model. The band gap energy is shown in Fig. 6 as a function of the strain. At the initial states, the band gap energy, E_{gap}, of the nanofilms is lower than that of the single crystal, and the thinner film has the lower gap. E_{gap} decreases with increasing tensile strain in all the models, and the strain at which the gap becomes null is higher in the thinner film. It is worth noting that the band gap in the thin film sustains up to higher tensile strain in spite of the lower band gap at the initial state than the bulk. Figure 7 shows changes in the band structure of the bulk and the 10-layer thin film under tension. The bulk has the indirect band gap structure at the initial state. This changes to a direct gap at $\varepsilon=0.01$ and the gap is closed at Γ. Surface states form a narrower indirect gap in the thin film and the film holds the indirect gap structure until the gap vanishes.

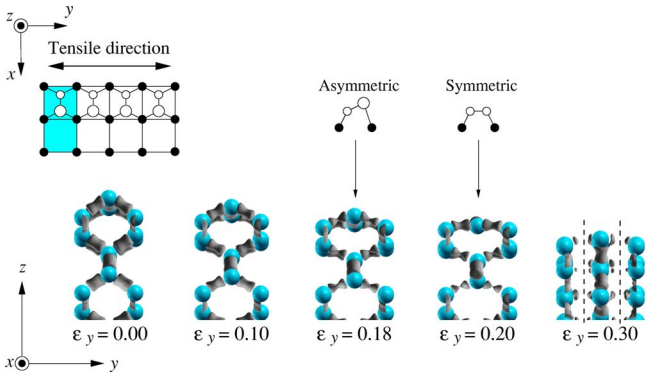

FIG. 5. (Color online) Change in atomic configuration and charge density distribution in Si nanofilms under $[0\bar{1}1]$ tension (14-layer model). Only the top half of the system is shown.

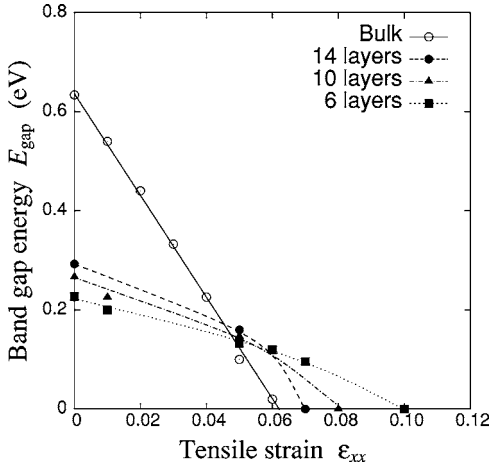

FIG. 6. Change in band gap energy of nanofilms and single crystal under tension.

IV. DISCUSSION

Equations (1) and (2) do not include $O(\varepsilon^2)$ terms of the surface stress contribution. This is justified because the surface energy is expressed well with a quadratic function, meaning that the contribution of the second-order term in the surface stress is negligible. On the other hand, the $O(\varepsilon^2)$ terms of the elastic stress of the bulk part should not be omitted. To obtain the surface stresses and its derivatives with regard to in-plane strain listed in Table I, we take the average of the values obtained from the three models. We found good agreement for the surface energy, γ, which is evaluated as 1.31 J/m^2 (in the literature one finds $\gamma=1.45$,[44] 1.38,[45] 1.21,[46] etc.). The surface stresses, f_{x0} and f_{y0}, also show good agreement with those in the literature[47] (in Table I). The two equations, Eqs. (1) and (2), are constructed for the energy balance in the x and y directions, respectively. t_0 evaluated by both the equations should be identical, thus we

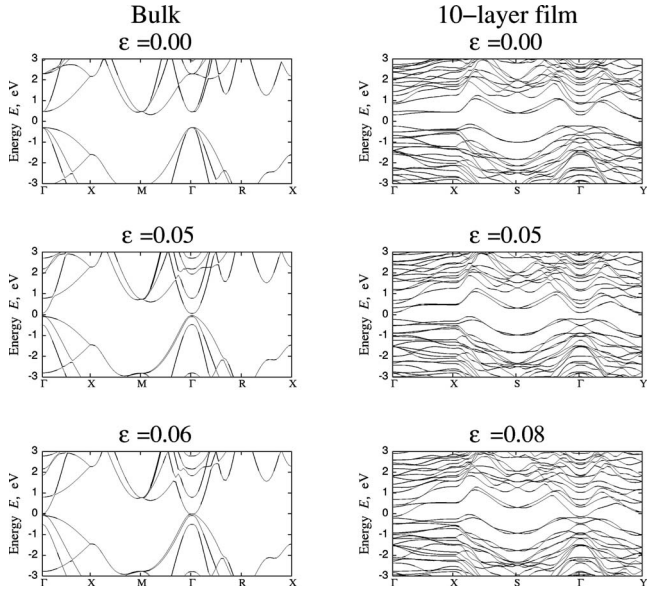

FIG. 7. Band configurations of nanofilms under tension.

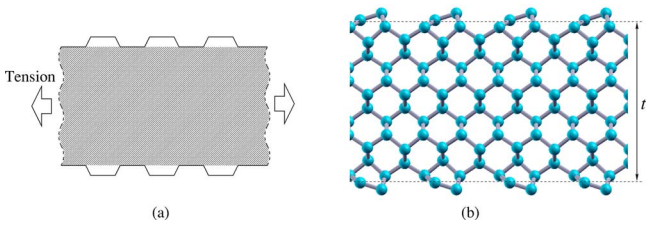

FIG. 8. (Color online) "Mechanical view" of thin films. (a) Schematic illustration: tensile stress is distributed to the shaded area. (b) Definition of the thickness of Si(100) film by a mechanical view.

can use both in principle. $(\partial f_y/\partial \varepsilon_y)_0$ and $(\partial f_y/\partial \varepsilon_x)_0$ are relatively less accurate, which is due to $|f_y|$ being considerably small. Therefore we used Eq. (1) instead of Eq. (2) to avoid undesirable error in the estimation of the thermodynamics thickness. Although more precise calculations with increased numbers of k points and plane waves would be required to reduce the deviation, we do not pursue this because it is out of the focus of the paper.

In the previous section we evaluated the stress using the definition of the thickness based on thermodynamics. However, this is a macroscopic view and lacks the conception of atomic structure of the surface. In fact, the thicknesses evaluated with the thermodynamic concept (Table II) are larger than the distance between the uppermost and lowermost atoms in the films (see Fig. 1). On the other hand, considering the atomic structure we can take a "mechanical view" on thin film strength. With the given reconstruction of the (100) surface, it is reasonable to assume that the dimerized surface layer does not contribute to strength and to regard the thin film structure, as schematically depicted in Fig. 8. That is, assuming that the stress is distributed only to the shaded area of the films. Accepting this, we estimate the thickness of the films excluding the dimer layers on the top and bottom. The obtained values are listed in Table II.

The stress of thin films under tension based on the mechanical view is then evaluated and shown in Fig. 9. Surprisingly, the curves of the films up to $\varepsilon=0.1$ are almost identical and close to that of the bulk. This means that the elastic properties of the interior of the film, excluding just the surface layer, are independent of the film thickness as long as the strain is not high. The existence of the surface does decrease the ideal strength but the effect is not large in the 14-layer film, the ideal strength of which is 15.2 GPa, only slightly lower than that of the bulk, 15.8 GPa. The ideal strength diminishes with decreasing film thickness (see Table IV). The decrease of the ideal strength in the extremely thin films under 1.5 nm thick can be explained by the fracture mechanism in Fig. 3, which is the only case where fracture occurs from bond thinning induced by the surface structure.

Based on the mechanical view, we found that the surface does not considerably weaken the tensile strength although the surface is not perfectly flat with the dimer structure. Both the unevenness of the surface shape and the particular electronic structure produced by dimer rows have little effect on the strength. This allows us to surmise that a Si(100) surface with another surface reconstruction, e.g., $c(4\times2)$, may hold high strains and lead to high strength as well. We can also

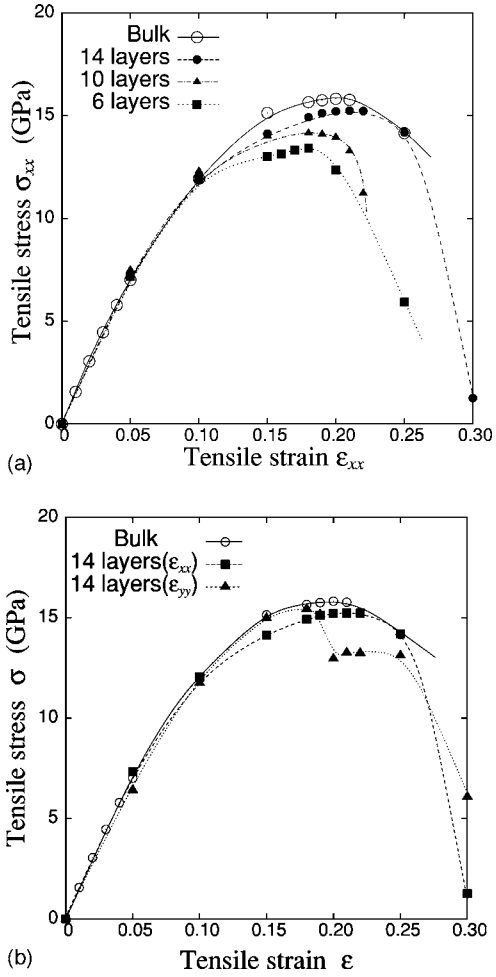

FIG. 9. Tensile stress-strain curves of Si nanofilms based on a mechanical view. (a) [011] tension. (b) $[0\bar{1}1]$ tension.

expect the strength of other closed packed surface orientations, e.g., Si(111), would not deviate much from that of the bulk. However, this would not necessarily be the case if the surface possesses a step, which causes a local stress field around the step edge leading to the decrease of the strength.[48]

Lehmann *et al.*[49] have carried out experiments of crack initiation at Si surfaces by means of the surface acoustic wave (SAW) technique and observed surface cracks nucleated on (111) planes. The estimated critical stresses for crack initiation are of the order of 1.6 GPa. This is significantly lower than the order of the ideal strength evaluated in the present work, indicating that the experimentally observed surface crack cannot be associated with a homogeneous crack nucleation from a clean surface. While the experimen-

TABLE IV. Ideal strength of thin films based on a mechanical view.

	Bulk	14-layer	10-layer	6-layer	14-layer
Tension	[011]	[011]	[011]	[011]	$[0\bar{1}1]$
Ideal strength	15.8 GPa	15.2	14.2	13.7	15.4

tal evaluation has been performed for H-terminated surfaces, it should be unreasonable to conjecture the surface type is responsible for the considerable difference in the critical stress. There must be substantial flaws, such as step structures, since instability of dimer structure alone does not much affect the ideal strength. The crack initiation with the low critical stress must rely on stress concentration caused by the surface flaws. Another experimental work has been published by Komai *et al.*,[50] reporting that the maximum fracture strength measured by bending tests of the single-crystal Si(110) microcantilever is 7.7 GPa. The fracture strength is still much lower than the ideal strength despite the experiment using well-polished microelements. They show the specimens possess surface roughness of 2 nm, which should be responsible for the low critical strength. Performing simulations for surfaces with flaws will be more relevant to explain the strength found in the experiments. However, there are numerous types of flaw to be concerned and investigating just several types will not be sufficient. Theoretical studies to cover a large variety of structures and defects are expected and will be our future task.

In the relaxed structure the band gap energy of the films are smaller than that of the bulk and the gap decreases with decreasing thickness. This may be explained as follows: While the ideal (100) surface has no band gap, dimerization by 2×1 relaxation causes Peierls distortion that opens up a gap between π and π^*. As the film gets thinner, the two dimerized surfaces start to interfere with each other electronically, resulting in incomplete Peierls distortion and a smaller gap. The vanishing of the band gap under tension stands for the conduction band descending to reach the Fermi energy level. In consequence the filling of the antibonding states takes place, which leads to weakening the stability of the bonding. This phenomenon, change in band configuration affecting the mechanical properties, has been discussed for other materials in some reports.[51,52] In the case of silicon it is expected that a discontinuity in the stress-strain relation would occur when the band gap vanishes because the occupancy of the conduction band suddenly becomes 1. However, it is not obvious in the present work and the stress-strain curves are rather smooth. In the case of a Si single crystal under shear, a smooth stress-strain relation has been reported.[28] In the calculation the occupancy changes rather smoothly due to the smearing band occupancy around the Fermi level to avoid divergence in the self-consistent loop, which can cover up a slight cusp. In any case a strong cusp in stress-strain curves is not expected.

It is well known that calculations based on DFT underestimate the band gap energy in spite of the use of GGA. In fact, the band gap obtained here for the bulk at the initial state is 0.63 eV, which is about half the experimentally observed value (1.17 eV). Assuming that the flaw of the theory does not deteriorate the qualitative evaluation, we estimate that the curves in the figure would be shifted upward, which suggest that the thin films hold the band gap up to larger tensile strain. However, a modified theory, such as LDA+U or GW approximation, would be necessary for a quantitative discussion on the band gap energy.

V. CONCLUSION

With the aim of obtaining fundamental knowledge of the influence of structure on mechanical properties, the ideal strengths of the Si nanofilms with (100) surfaces in $\langle011\rangle$ tension are obtained theoretically with *ab initio* simulations by means of the ultrasoft pseudopotential methodology with GGA. The ideal strength decreases only slightly with decreasing film thickness and little effect is found on the Young's modulus, meaning the surface as such is not much weaker than bulk. The presence of a flat surface does not decrease the ideal strength significantly unless one goes to extremely thin films under the thickness of 1 nm.

We found little difference in the ideal strength between [011] tension and $[0\bar{1}1]$, perpendicular and parallel to the arrangement of the dimer rows respectively, which indicates that the instability of the dimer structure alone does not much decrease the strength. We can speculate that Si(100) flat surfaces possess high strength unless substantial flaws in structure such as steps producing a stress concentration are introduced.

The thin films hold the band gap energy up to the higher tensile strain than the bulk, although the initial band gap in the films is smaller. While the band structure due to the presence of the surface has little influence on the mechanical property, the electronic property in the thin film under tension is much affected by the surface states. Although we cannot make a quantitative discussion about the band gap due to the use of DFT, our results give interesting insight to the electronic property of thin film under deformation.

ACKNOWLEDGMENT

This study was partly supported by the Center of Excellence for Research and Education on Complex Functional Mechanical Systems (COE program of the Ministry of Education, Culture, Sports, Science and Technology, Japan).

*Electronic address: umeno@kues.kyoto-u.ac.jp

[1] R. Phillips, *Crystals, Defects and Microstructures: Modeling Across Scales* (Cambridge University Press, Cambridge, 2001).
[2] M. Orriz, A. M. Cuitiño, J. Knap, and M. Koslowski, MRS Bull. **26** (3), 216 (2001).
[3] J. Li, A. H. W. Ngan, and P. Gumbsch, Acta Mater. **51**, 5711 (2003).
[4] A. E. Mattsson, P. A. Schultz, M. P. Desjarlais, T. R. Mattsson, and K. Leung, Modell. Simul. Mater. Sci. Eng. **13**, R1 (2005).
[5] P. Gumbsch, Mater. Sci. Eng., A **319**, 1 (2001).
[6] S. Yip, Nat. Mater. **2**, 3 (2003).
[7] V. E. Gorisenko, S. V. Gaponenko, and V. S. Gurin, *Physics, Chemistry and Application of Nanostructures* (World Scientific, Singapore, 2001).

[8] H. S. Nalwa, *Nanostructured Materials and Nanotechnology* (Academic Press, New York, 2002).
[9] M. Born and K. Huang, *Dynamical Theory of Crystal Lattices* (Oxford University Press, Oxford, 1954).
[10] F. Milstein, Phys. Rev. B **3**, 1130 (1971).
[11] R. Hill and F. Milstein, Phys. Rev. B **15**, 3087 (1977).
[12] M. Tang and S. Yip, J. Appl. Phys. **76**, 2719 (1994).
[13] J. Wang, S. Yip, S. R. Phillpot, and D. Wolf, Phys. Rev. Lett. **71**, 4182 (1993).
[14] J. Wang, S. Yip, S. Phillpot, and D. Wolf, Phys. Rev. B **52**, 12627 (1995).
[15] J. Wang, J. Li, S. Yip, D. Wolf, and S. Phillipot, Physica A **240**, 396 (1997).
[16] L. G. Wang and M. Šob, Phys. Rev. B **60**, 844 (1999).
[17] W. Li and T. Wang, J. Phys.: Condens. Matter **10**, 9889 (1998).
[18] W. Li and T. Wang, Phys. Rev. B **59**, 3993 (1999).
[19] S. Subramanian and S. Yip, Comput. Mater. Sci. **23**, 116 (2002).
[20] J. Li, K. J. Van Vliet, T. Zhu, S. Yip, and S. Suresh, Nature **418**, 307 (2002).
[21] S. Yip, J. Li, M. Tang, and J. Wang, Mater. Sci. Eng., A **317**, 236 (2001).
[22] K. Mizushima, S. Yip, and E. Kaxiras, Phys. Rev. B **50**, 14952 (1994).
[23] S. Ogata, J. Li, and S. Yip, Science **298**, 807 (2002).
[24] M. Šob, L. Wang, and V. Vitek, Mater. Sci. Eng., A **234–236**, 1075 (1997).
[25] P. Šandera, J. Pokluda, L. Wang, and M. Šob, Mater. Sci. Eng., A **234–236**, 370 (1997).
[26] D. Clatterbuck, D. Chrzan, and J. Morris, Jr., Acta Mater. **51**, 2271 (2003).
[27] D. Roundy and M. Cohen, Phys. Rev. B **64**, 212103 (2001).
[28] Y. Umeno and T. Kitamura, Mater. Sci. Eng., B **88**, 79 (2002).
[29] G. Kresse and J. Hafner, Phys. Rev. B **47**, 558 (1993).
[30] G. Kresse and J. Furthmüller, Phys. Rev. B **54**, 11169 (1996).
[31] P. Hohenberg and W. Kohn, Phys. Rev. **136**, B864 (1964).
[32] W. Kohn and L. Sham, Phys. Rev. **140**, A1133 (1965).
[33] K. Ohno, K. Esfarjani, and Y. Kawazoe, *Computational Materials Science: From Ab Initio to Monte Carlo Methods* (Springer-Verlag, Berlin, 1999), p. 77.
[34] D. Vanderbilt, Phys. Rev. B **41**, 7892 (1990).
[35] J. Perdew and Y. Wang, Phys. Rev. B **45**, 13244 (1992).
[36] B. G. Streetman, *Solid State Electronic Devices*, 3rd ed. (Prentice–Hall, Englewood Cliffs, NJ, 1990).
[37] E. Ericson *et al.*, "Mechanical properties of materials in microstructure," *Handbook of Micro/Nanotechnology* (CRC Press LLC, Florida, 1999).
[38] H. J. McSkimin, J. Appl. Phys. **24**, 988 (1953).
[39] H. J. McSkimin and P. Andreatch, Jr., J. Appl. Phys. **35**, 3312 (1964).
[40] H. Monkhorst and J. Pack, Phys. Rev. B **13**, 5188 (1976).
[41] A. Kokalj, J. Mol. Graphics Modell. **17**, 176 (1999).
[42] R. C. Cammarata and K. Sieradzki, Phys. Rev. Lett. **62**, 2005 (1989).
[43] R. Cammarata, Prog. Surf. Sci. **46**, 1 (1994).
[44] A. A. Stekolnikov, J. Furthmüller, and F. Bechstedt, Phys. Rev. B **65**, 115318 (2002).
[45] S. C. Erwin, A. A. Baski, and L. J. Whitman, Phys. Rev. Lett. **77**, 687 (1996).
[46] T. Takai, T. Halicioglu, and W. A. Tiller, Surf. Sci. **164**, 327 (1985).
[47] Y. Miyamoto, Phys. Rev. B **49**, 1947 (1994).
[48] A. Koma, K. Yagi, M. Tsukada, and M. Aono, *Introduction to Surface Science* (Maruzen Ltd., Tokyo, 1994) (in Japanese).
[49] G. Lehmann, A. Lomonosov, P. Hess, and P. Gumbsch, J. Appl. Phys. **94**, 2907 (2003).
[50] K. Komai, K. Minoshima, and S. Inoue, Microsyst. Technol. **5**, 30 (1998).
[51] T. Li, J. Morris, and D. Chrzan, Phys. Rev. B **70**, 054107 (2004).
[52] J. Gilman, Science **274**, 65 (1996).